Anomalous tumbling of colloidal ellipsoids in Poiseuille flows

Lauren E. Altman,[1,2] Andrew D. Hollingsworth,[1] and David G. Grier[1]
[1]*Department of Physics and Center for Soft Matter Research, New York University, New York, New York 10003, USA*
[2]*Department of Physics and Astronomy, University of Pennsylvania, Philadelphia, Pennsylvania 19104, USA*

(Received 22 May 2023; accepted 6 September 2023; published 28 September 2023)

Shear flows cause aspherical colloidal particles to tumble so that their orientations trace out complex trajectories known as Jeffery orbits. The Jeffery orbit of a prolate ellipsoid is predicted to align the particle's principal axis preferentially in the plane transverse to the axis of shear. Holographic microscopy measurements reveal instead that colloidal ellipsoids' trajectories in Poiseuille flows strongly favor an orientation inclined by roughly $\pi/8$ relative to this plane. This anomalous observation is consistent with at least two previous reports of colloidal rods and dimers of colloidal spheres in Poiseuille flow and therefore appears to be a generic, yet unexplained feature of colloidal transport at low Reynolds numbers.

DOI: 10.1103/PhysRevE.108.034609

I. INTRODUCTION

Dispersions of aspherical colloidal particles flow differently than dispersions of spheres because shear forces cause aspherical particles to tumble [1,2] and tumbling influences interparticle interactions [3]. How shear-mediated tumbling affects colloidal transport has ramifications for such diverse application areas as filtration [4], drug delivery [5], and food processing [6]. Tumbling also influences the behavior of active particles that propel themselves through shear flows, including motile bacteria and artificial swimmers [7–10]. Despite more than a century of study, the kinematics of colloidal tumbling are incompletely understood, even for comparatively simple particle shapes and flow profiles, and even when inertial and viscoelastic effects may be ignored.

The present study uses holographic video microscopy to explore anomalous tumbling of axisymmetric ellipsoids in simple shear flows. Such particles are predicted [1,2,11] to align preferentially in the plane transverse to the shear direction. Recent experimental studies, however, show that colloidal rods [12] and bound pairs of colloidal spheres [13] tend instead to be inclined at $\theta \approx \pi/8$ relative to the predicted plane when they are entrained in plane Poiseuille flows. Here, we show that prolate colloidal ellipsoids also tend to be anomalously inclined in steady Poiseuille flows, in quantitative agreement with previous experimental studies [12,13] and in qualitative disagreement with theoretical predictions.

II. JEFFERY ORBITS IN POISEUILLE FLOWS

Figure 1 schematically depicts the system used for this study. A nonaqueous dispersion of colloidal ellipsoids is transported down a rectangular channel by a pressure-driven flow. Particles in the stream pass through a collimated laser beam. The light they scatter interferes with the rest of the beam in the focal plane of a microscope that magnifies the interference pattern and relays it to a camera. The image in Fig. 1 is a region of interest from a typical video frame that captures the hologram of one ellipsoidal particle. Such holograms can be analyzed to estimate the inclination angle, θ, for each particle passing through the observation volume [13].

In the absence of shear, a colloidal ellipsoid would undergo free rotational diffusion, with its orientational unit vector tracing out a random walk on the unit sphere. The associated distribution of observed inclination angles is

$$P_0(\theta) = \cos(\theta) \tag{1}$$

over the experimentally accessible domain, $\theta \in [0, \pi/2]$. This distribution is peaked at $\theta = 0$, which means that the ellipsoid is most likely to be observed with its major axis aligned with the observation plane.

The Poiseuille flow profile in the channel has a height-dependent shear rate, $\dot{\gamma}(z) = -8v_0 z/H^2$, that causes the ellipsoids to tumble as they travel downstream (along $\hat{x}$). For convenience, we define $z = 0$ to lie along the midplane of the channel, where the flow speed is v_0. The flow's vorticity is directed along $\hat{y}$. For simplicity, we assume that the height of the channel, H, is large enough compared to particles' dimensions that the shear may be treated as if it were uniform across the volume of a particle.

When subjected to a uniform shear flow, an axisymmetric ellipsoid traces out a Jeffery orbit that is most naturally expressed in terms of the polar angle, θ', relative to the axis of vorticity, $\hat{y}$, and the azimuthal angle, ϕ', around that axis. We adopt the convention that $\phi' = 0$ is aligned with the gradient direction, $\hat{z}$. The experimentally accessible angle of inclination, θ, is related to θ' and ϕ' by

$$\sin\theta = \sin\theta' \cos\phi'. \tag{2}$$

Neglecting both inertial effects and diffusion, the orientation of a tumbling ellipsoid is predicted [1,11] to trace out a trajectory, $[\theta'(t), \phi'(t)]$, that is described by

$$\tan\phi'(t) = \lambda \tan(\Omega t), \tag{3a}$$

$$\tan\theta'(t) = \frac{C\lambda}{(\lambda^2\cos^2\phi' + \sin^2\phi')^{1/2}}, \tag{3b}$$

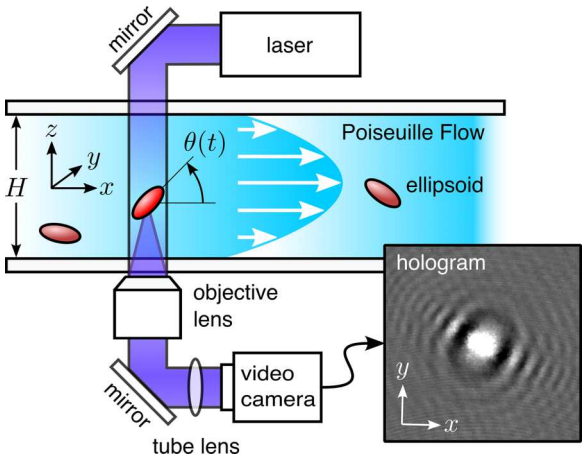

FIG. 1. Schematic representation of colloidal ellipsoids tumbling as they are transported by the Poiseuille flow in a microfluidic channel. The particles' positions and orientations are recorded by an in-line holographic microscope that illuminates them with a collimated laser beam. Light scattered by an ellipsoid interferes with the remainder of the beam in the microscope's focal plane. The magnified intensity pattern is recorded by a video camera. A region of interest from one such video frame captures the hologram of a typical ellipsoid and can be analyzed using the Lorenz-Mie theory of light scattering to measure the ellipsoid's three-dimensional orientation.

where $\lambda = a/b$ is the ratio of the major axis, a, to the minor axis, b. The orientational trajectory is periodic with a frequency

$$\Omega = \frac{\lambda}{1+\lambda^2}\,\dot{\gamma} \tag{3c}$$

that depends on the shear rate and the ellipsoid's aspect ratio. Different orbits are distinguished by the orbital constant, C. Values around $C = 0$ correspond to log-rolling motion in which the ellipsoid's major axis is oriented predominantly along $\hat{y}$, so that $\theta \approx 0$. Large values of C correspond to a cartwheeling motion in which the ellipsoid tumbles with its major axis predominantly in the x-z plane. Even in this limit, the ellipsoid is most likely to be observed near $\theta = 0$ because its orientation advances most slowly as the major axis passes through the x-y plane. More generally, the distribution of observed orientation angles, $P(\theta|C)$, is peaked at $\theta \ll \pi/8$ for all values of C.

Rotational diffusion causes a Brownian ellipsoid's trajectory to wander stochastically among orbits with different values of C [14]. A slender ellipsoid in a simple shear flow, for example, has values of C drawn from the probability distribution [15,16],

$$p(C) = \frac{4RC}{(4RC^2+1)^{3/2}}, \tag{4}$$

where R is the ratio of the ellipsoid's rotational diffusion coefficients and therefore depends on λ. Weak inertial effects at nonvanishing rotational Reynolds numbers destabilize log-rolling and stabilize cartwheeling, favoring larger values of C than is predicted by Eq. (4) [17–19]. The thermally averaged distribution of inclination angles follows as

$$P(\theta) = \int_0^\infty P(\theta|C)\,p(C)\,dC \tag{5}$$

and is peaked at $\theta = 0$ because $P(\theta|C)$ is peaked near $\theta = 0$ and $p(C) > 0$. We conclude from this that the observed distribution of orientation angles should be peaked at $\theta = 0$, regardless of the form of $p(C)$ and independent of the shear rate, $\dot{\gamma}$. Surprisingly, this does not appear to be consistent with experimental observations [12,13], including those reported here.

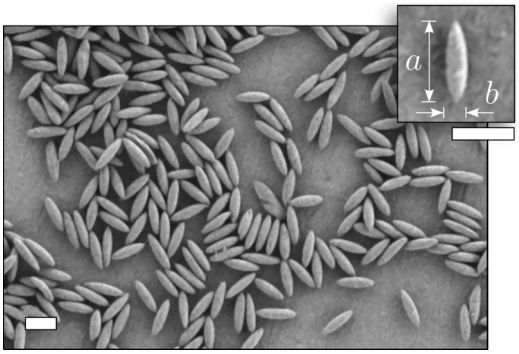

FIG. 2. Scanning electron microscope image of colloidal ellipsoids deposited onto a graphite substrate and dried. Inset: typical ellipsoid, illustrating ground-truth measurement of the major and minor axes, a and b, respectively. Scale bars indicate 5 μm.

III. HOLOGRAPHIC TRACKING OF COLLOIDAL ELLIPSOIDS

The monodisperse colloidal ellipsoids used for this study are created by uniformly stretching [20,21] custom-synthesized polymethyl methacrylate spheres (NYU Colloid Synthesis Facility, batch CSF02-139-C) [22,23]. Scanning electron microscopy images such as the example in Fig. 2 yield a population-averaged major axis of $a = (4.80 \pm 0.21)\,\mu\text{m}$ and an aspect ratio $\lambda = 3.96 \pm 0.25$. As has been reported previously [24], stretched colloidal spheres differ slightly in shape from ideal ellipsoids. They are closer to ideal, however, than the right-circular rods [12] and bound pairs of spheres [13] that have been studied previously.

Sterically stabilized colloidal ellipsoids are dispersed in dodecane ($n_m = 1.42$) at a concentration of 10^6 particles mL^{-1}. A 30 μL aliquot is transferred to the input reservoir of a commercial microfluidic channel (xCell8, Spheryx, Inc.) with a rectangular cross section that nominally is $H = 60\,\mu\text{m}$ high and and 500 μm wide. The 10:1 aspect ratio allows us to neglect transverse shear. The microfluidic channel is installed in a commercial holographic particle characterization instrument (xSight, Spheryx, Inc.) that creates a pressure-driven flow in the channel with a nominal midplane speed of $v_0 = 3\,\text{mm s}^{-1}$.

The instrument analyzes each single-particle hologram [25] with the Lorenz-Mie theory of light scattering [26–28] to obtain the diameter, d_p^*, and refractive index, n_p^*, that describes an effective sphere encompassing the particle [13,29–31]. These effective-sphere parameters are related

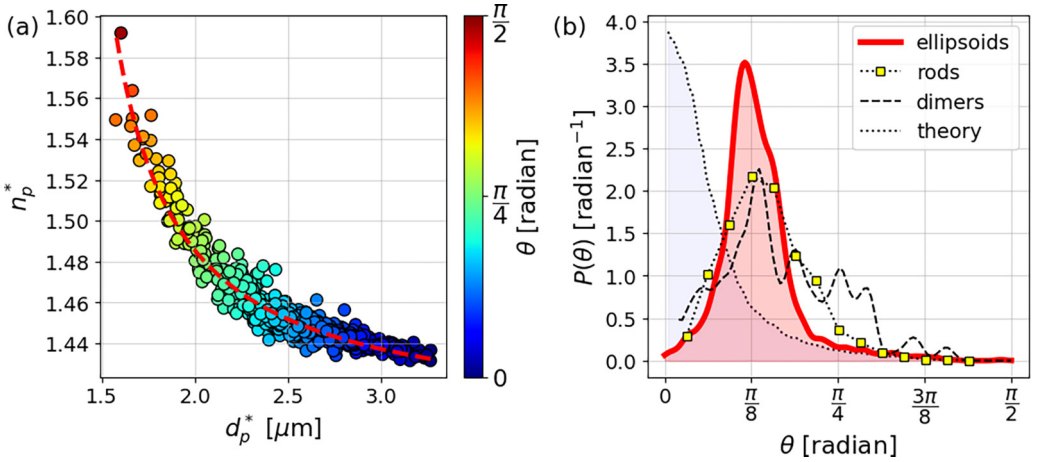

FIG. 3. (a) Effective-sphere properties of 1712 colloidal ellipsoids, with each point representing the holographically measured diameter, d_p^*, and refractive index, n_p^*, of a single particle. The dashed (red) curve is a fit to Eq. (6). Each data point is colored by the angle of inclination, θ, associated with its position along the parametric curve. (b) Distribution of ellipsoid inclination angles, $P(\theta)$, obtained from the data in (a), compared with independent results for colloidal rods [12] and dimers [13]. The theoretical prediction for Brownian ellipsoids is obtained from Eqs. (3) through (5).

to an ellipsoid's angle of inclination through Maxwell Garnett effective-medium theory [32]. An ellipsoid lying in the focal plane, $\theta = 0$, has an effective diameter somewhat smaller than its major axis. Because the actual ellipse fills only a fraction of this enclosing sphere, however, its effective refractive index in this orientation is only slightly greater than that of the medium [13]. An ellipsoid aligned with the optical axis, $\theta = \pi/2$, scatters light in much the same way as a small dense sphere. The dependence of effective properties on ellipsoid orientation is captured by the phenomenological relationship [13]

$$d_p^*(\theta) = (d_{\min} - d_{\max})\sin\theta + d_{\max}, \tag{6a}$$

$$n_p^*(\theta) = n_0\left[1 + \frac{L}{d_p^*(\theta) - d_0}\right], \tag{6b}$$

where $d_{\max} = 3.27\,\mu\text{m}$ and $d_{\min} = 1.57\,\mu\text{m}$ are the maximum and minimum observed values of d_p^*. Figure 3(a) presents experimental results for 1712 colloidal ellipsoids obtained from the sample in Fig. 2. Each data point reflects the effective diameter and refractive index of a single ellipsoid captured at a random point in its orientational trajectory. The (red) dashed curve is a fit of those data points to Eq. (6b) for $L = (65 \pm 2)\text{nm}$, $d_0 = (1.24 \pm 0.01)\,\mu\text{m}$, and $n_0 = 1.40$. The points then are colored according to the inclination angle, θ, of the closest point along that curve.

The random sampling of inclination angles in Fig. 3(a) is compiled into a probability distribution $P(\theta)$ that is plotted in Fig. 3(b). Whereas the theory summarized in Eqs. (3) through (5) predicts that Brownian ellipsoids are most likely to be aligned with the imaging plane, $\theta = 0$, the measured distribution is clearly peaked around $\theta = \pi/8$. The same anomalous inclination has been observed in measurements on colloidal dimers [13] and colloidal rods [12], both of which are reproduced in Fig. 3(b).

The qualitative discrepancy between the predicted and observed distribution of inclination angles was noted in [12] and was emphasized in [13]. This discrepancy is unlikely to result from an experimental artifact because the same result is obtained with orthogonal measurement techniques [12,13].

Lacking a definitive explanation for the observed anomalous inclination, we review factors that are not included in the standard formulation of Jeffery orbits that might affect tumbling transport of aspherical particles in Poiseuille flows. Figure 4(a) reports the axial position, z_p, and in-plane flow speed, v_p, for each particle from Fig. 3(a). The (yellow) dashed curve is a fit to the parabolic Poiseuille flow profile. The resulting estimates for the channel height, $H = (63 \pm 1)\,\mu\text{m}$, and midplane flow speed, $v_0 = (3.5 \pm 0.2)\text{mm s}^{-1}$, are consistent with the instrument's specifications. The shear rate experienced by the ellipsoids ranges from $\dot{\gamma} = 0$ at the midplane to $\dot{\gamma} \gtrsim 100\,\text{s}^{-1}$ near the walls. The associated rotational Péclet number therefore varies from zero on the midplane to roughly 200 near the walls. In this regime, the ellipsoids' orientational trajectories should be dominated by kinematics rather than by rotational diffusion throughout most of the height of the channel.

The channel's height is sufficiently large compared with the ellipsoids' major axis ($H > 10a$) that gradients in the shear rate should not influence the rotational kinematics of individual ellipsoids beyond creating a distribution of orbital periods [33,34]. Recently reported Brownian dynamics simulations on colloidal rods in comparable Poiseuille flows [12] confirm the prediction [16] that $P(\theta)$ should be peaked at $\theta = 0$, rather than at $\theta = \pi/8$ as is observed experimentally.

The ellipsoids' shear Reynolds number in dodecane is smaller than $\text{Re}_s = 3 \times 10^{-4}$. Although small, this may still be large enough for weak inertial effects to have destabilized log-rolling trajectories near $\theta = 0$ [18]. The resulting increase in relative probability at steeper inclinations would be apparent in the random sampling of orientations that is captured by our measurement technique. Because Re_s is small, however, this effect seems unlikely to suppress $P(\theta)$ near $\theta = 0$ to the extent that is observed experimentally in Fig. 3(b).

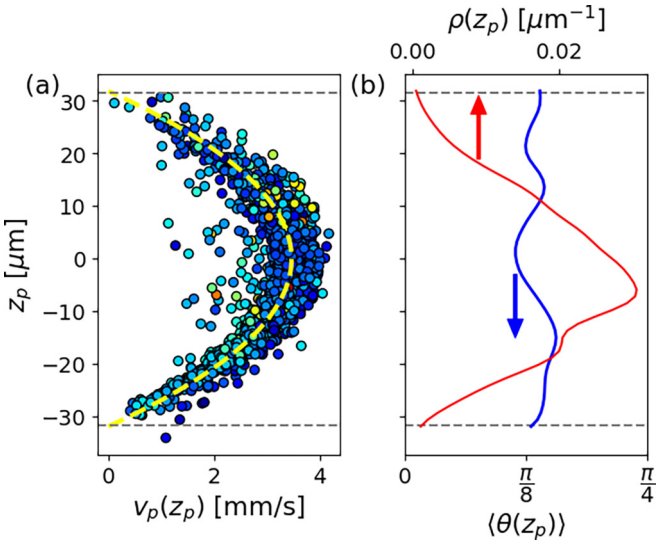

FIG. 4. (a) Holographic tracking data obtained simultaneously with characterization results from Fig. 3(a). Each point indicates the axial position, z_p, and the flow speed, v_p, of a single particle and is colored by the inclination angle from Fig. 3(a). The dashed (yellow) curve is a fit to the parabolic Poiseuille flow profile with a maximum speed of $v_0 = 3.5\,\mathrm{mms}^{-1}$ at the midplane. Dashed (gray) lines represent estimates for the axial positions of the channel walls. Their separation, $H = (63 \pm 1)\,\mu\mathrm{m}$, is obtained from the fit. (b) The population-average inclination angle, $\langle\theta(z_p)\rangle$, does not depend significantly on the ellipsoids' height in the channel (blue curve) even though the probability distribution for particle positions, $\rho(z_p)$ (red curve), shows a clear tendency for ellipsoids to travel near the channel's midplane.

Hydrodynamic coupling to the walls of the channel also may have influenced the ellipsoids' trajectories [35]. This could explain the nonuniform distribution of axial positions, $\rho(z_p)$, that is plotted in Fig. 4(b). Redistribution of particles away from the channel's walls and toward the midplane may be a manifestation of hydrodynamic lift [36,37]. Hydrodynamic coupling to the walls might also have a complementary effect on the ellipsoids' orientational trajectories. Any coupling-induced orientational bias appears to depend weakly on position within the channel, however, because the mean inclination angle, plotted in Fig. 4(b), has no obvious dependence on z_p.

IV. DISCUSSION

The trajectories of axisymmetric colloidal particles in simple shear flows continue to present conundrums despite more than a century of study. Holographic particle characterization offers a fast and effective way to amass large statistical samples that hopefully will be useful for resolving some of these outstanding mysteries. Analyzing holographic particle-characterization data in the effective-sphere approximation yields useful estimates for elliptical particles' out-of-plane orientations. The same measurement also yields each particle's position in the three-dimensional flow over a comparatively large axial range, as well as the drift speed at that position.

Holographic tracking of tumbling ellipsoids confirms previous reports that aspherical colloids do not behave as expected in plane Poiseuille flows. Rather than spending most of their time in the plane defined by the flow and vorticity directions, these particles actually tend to be inclined away from that plane. The same angle of inclination, $\theta = \pi/8$, is adopted by dimers with an aspect ratio of 2 [13], rods with an aspect ratio as large as 10 [12], and ellipsoids with an aspect ratio of 5. The angle of inclination appears not to depend strongly on the particles' distance from bounding walls, even when the particles themselves experience significant hydrodynamic lift. Interparticle collisions similarly are not likely to account for these anomalous observations because the typical interparticle separation exceeds the channel height in all available studies.

ACKNOWLEDGMENTS

The work at New York University was supported by the National Science Foundation through Award No. DMR-2104837. The xSight holographic particle characterization instrument was acquired as shared instrumentation with support from the MRSEC program of the NSF under Award No. DMR-1420073. The Merlin FESEM was acquired through the support of the MRI program of the NSF under Award No. DMR-0923251. We are grateful to A. Y. Grosberg and A. Donev for helpful conversations regarding Jeffery orbits. We also appreciate useful comments from A. Zumbusch regarding the ellipsoidal particle synthesis.

D.G.G. is a founder of Spheryx, Inc., the company that manufactures the instrument for holographic particle characterization that was used in this study.

[1] G. B. Jeffery, The motion of ellipsoidal particles immersed in a viscous fluid, Proc. R. Soc. London A **102**, 161 (1922).
[2] F. P. Bretherton, The motion of rigid particles in a shear flow at low Reynolds number, J. Fluid Mech. **14**, 284 (1962).
[3] E. Hinch and L. Leal, The effect of Brownian motion on the rheological properties of a suspension of non-spherical particles, J. Fluid Mech. **52**, 683 (1972).
[4] M. B. Salerno, M. Flamm, B. E. Logan, and D. Velegol, Transport of rodlike colloids through packed beds, Environ. Sci. Technol. **40**, 6336 (2006).
[5] E. Blanco, H. Shen, and M. Ferrari, Principles of nanoparticle design for overcoming biological barriers to drug delivery, Nat. Biotech. **33**, 941 (2015).
[6] E. Dickinson, Colloids in food: Ingredients, structure, and stability, Annu. Rev. Food Sci. Techn. **6**, 211 (2015).
[7] G. Junot, N. Figueroa-Morales, T. Darnige, A. Lindner, R. Soto, H. Auradou, and E. Clément, Swimming bacteria in Poiseuille flow: The quest for active Bretherton-Jeffery trajectories, Europhys. Lett. **126**, 44003 (2019).
[8] K. Ishimoto, Jeffery's orbits and microswimmers in flows: A theoretical review, J. Phys. Soc. Jpn. **92**, 062001 (2023).
[9] T. Omori, K. Kikuchi, M. Schmitz, M. Pavlovic, C.-H. Chuang, and T. Ishikawa, Rheotaxis and migration of an unsteady microswimmer, J. Fluid Mech. **930**, A30 (2022).
[10] R. Baker, J. E. Kauffman, A. Laskar, O. E. Shklyaev, M. Potomkin, L. Dominguez-Rubio, H. Shum, Y. Cruz-Rivera,

I. S. Aranson, A. C. Balazs *et al.*, Fight the flow: the role of shear in artificial rheotaxis for individual and collective motion, Nanoscale **11**, 10944 (2019).

[11] P. Saffman, On the motion of small spheroidal particles in a viscous liquid, J. Fluid Mech. **1**, 540 (1956).

[12] A. Zöttl, K. E. Klop, A. K. Balin, Y. Gao, J. M. Yeomans, and D. G. Aarts, Dynamics of individual Brownian rods in a microchannel flow, Soft Matter **15**, 5810 (2019).

[13] L. E. Altman, R. Quddus, F. C. Cheong, and D. G. Grier, Holographic characterization and tracking of colloidal dimers in the effective-sphere approximation, Soft Matter **17**, 2695 (2021).

[14] E. J. Hinch and L. G. Leal, Rotation of small non-axisymmetric particles in a simple shear flow, J. Fluid Mech. **92**, 591 (1979).

[15] M. Rahnama, D. L. Koch, Y. Iso, and C. Cohen, Hydrodynamic, translational diffusion in fiber suspensions subject to simple shear flow, Phys. Fluids A **5**, 849 (1993).

[16] M. Rahnama, D. L. Koch, and E. S. Shaqfeh, The effect of hydrodynamic interactions on the orientation distribution in a fiber suspension subject to simple shear flow, Phys. Fluids **7**, 487 (1995).

[17] J. Einarsson, F. Candelier, F. Lundell, J. R. Angilella, and B. Mehlig, Rotation of a spheroid in a simple shear at small Reynolds number, Phys. Fluids **27**, 063301 (2015).

[18] J. Einarsson, F. Candelier, F. Lundell, J. R. Angilella, and B. Mehlig, Effect of weak fluid inertia upon Jeffery orbits, Phys. Rev. E **91**, 041002(R) (2015).

[19] D. Palanisamy and W. K. den Otter, Intrinsic viscosities of nonspherical colloids by Brownian dynamics simulations, J. Chem. Phys. **151**, 184902 (2019).

[20] A. Mohraz and M. J. Solomon, Direct visualization of colloidal rod assembly by confocal microscopy, Langmuir **21**, 5298 (2005).

[21] M. K. Klein, A. Zumbusch, and P. Pfleiderer, Photocrosslinkable, deformable PMMA colloids, J. Mater. Chem. C **1**, 7228 (2013).

[22] L. Antl, J. Goodwin, R. Hill, R. H. Ottewill, S. Owens, S. Papworth, and J. Waters, The preparation of poly (methyl methacrylate) latices in non-aqueous media, Colloids Surf. **17**, 67 (1986).

[23] M. T. Elsesser and A. D. Hollingsworth, Revisiting the synthesis of a well-known comb-graft copolymer stabilizer and its application to the dispersion polymerization of poly (methyl methacrylate) in organic media, Langmuir **26**, 17989 (2010).

[24] J. A. Ferrar, L. Pavlovsky, E. Viges, Y. Liu, and M. J. Solomon, Two-step continuous production of monodisperse colloidal ellipsoids at rates of one gram per day, AIChE J. **64**, 697 (2018).

[25] S.-H. Lee, Y. Roichman, G.-R. Yi, S.-H. Kim, S.-M. Yang, A. van Blaaderen, P. van Oostrum, and D. G. Grier, Characterizing and tracking single colloidal particles with video holographic microscopy, Opt. Express **15**, 18275 (2007).

[26] C. F. Bohren and D. R. Huffman, *Absorption and Scattering of Light by Small Particles* (Wiley Interscience, New York, 1983).

[27] M. I. Mishchenko, L. D. Travis, and A. A. Lacis, *Scattering, Absorption, and Emission of Light by Small Particles* (Cambridge University Press, Cambridge, UK, 2002).

[28] G. Gouesbet and G. Gréhan, *Generalized Lorenz-Mie Theories* (Springer-Verlag, Berlin, 2011), Vol. 31.

[29] M. A. Odete, F. C. Cheong, A. Winters, J. J. Elliott, L. A. Philips, and D. G. Grier, The role of the medium in the effective-sphere interpretation of holographic particle characterization data, Soft Matter **16**, 891 (2020).

[30] L. E. Altman and D. G. Grier, Interpreting holographic molecular binding assays with effective medium theory, Biomed. Opt. Express **11**, 5225 (2020).

[31] R. Abdulali, L. E. Altman, and D. G. Grier, Multi-angle holographic characterization of individual fractal aggregates, Opt. Express **30**, 38587 (2022).

[32] V. A. Markel, Introduction to the Maxwell Garnett approximation: tutorial, J. Opt. Soc. Am. A **33**, 1244 (2016).

[33] A. T. Chwang, Hydromechanics of low-Reynolds-number flow. Part 3. Motion of a spheroidal particle in quadratic flows, J. Fluid Mech. **72**, 17 (1975).

[34] C. A. Stover and C. Cohen, The motion of rodlike particles in the pressure-driven flow between two flat plates, Rheol. Acta **29**, 192 (1990).

[35] D. Schiby and I. Gallily, On the orderly nature of the motion of nonspherical aerosol particles. III. The effect of the particle-wall fluid-dynamic interaction, J. Colloid Interface Sci. **77**, 328 (1980).

[36] R. Ouchene, M. Khalij, A. Tanière, and B. Arcen, Drag, lift and torque coefficients for ellipsoidal particles: From low to moderate particle Reynolds numbers, Comput. Fluids **113**, 53 (2015).

[37] J. Bagge, T. Rosén, F. Lundell, and A.-K. Tornberg, Parabolic velocity profile causes shape-selective drift of inertial ellipsoids, J. Fluid Mech. **926**, A24 (2021).